Plastic deformation in Al (Cu) interconnects stressed by electromigration and studied by synchrotron polychromatic X-ray microdiffraction

Kai Chen[1,2], N. Tamura[1], B. C. Valek[1] and K. N. Tu[2]

1 Advanced Light Source, Lawrence Berkeley National Laboratory, 1 Cyclotron Rd, Berkeley, CA 94720

2 Dept. of Materials Science and Engineering, UCLA, Los Angeles, CA 90095

Abstract

We report here an in-depth synchrotron radiation based white beam X-ray microdiffraction study of plasticity in individual grains of an Al (Cu) interconnect during the early stage of electromigration. The study shows a rearrangement of the geometrically necessary dislocations (GND) in bamboo typed grains during that stage. We find that about 90% of the GNDs are oriented so that their line direction is the closest to the current flow direction. In non-bamboo typed grains, the Laue peak positions shift, indicating that the grains rotate. An analysis in terms of force directions has been carried out and is consistent with observed electromigration induced grain rotation and bending.

I. Introduction

Electromigration (EM) is a physical phenomenon that may lead to integrated circuit failure by void formation at the cathode end or extrusion at the anode end of interconnects that connect the millions of transistors in the circuit on a Si chip. This deleterious phenomenon becomes more severe with the trend of miniaturization of electronic devices [1]. In very-large-scale integration (VLSI) of circuits on a Si device, Al or Cu thin-film line can experience a current density that reaches or exceeds 10^6 A/cm^2, causing electromigration in the line at the device working temperature. This may lead to void formation at the cathode and extrusion at the anode end if a crack forms in the passivation layer, causing failure by respectively open circuit or short circuit [2]. Because of the interest in the effect of failure on device performance, most studies on electromigration have been concentrated on microstructure changes at the cathode and the anode. Much less has been studied in regions between the cathode and the anode. As the size of the electronic devices keeps on decreasing, the practical significance of electromigration effect on interconnects becomes even more important. Much research has been conducted and many models have been proposed [3-6]. While the general mechanism of electromigration is understood, the effect of the atomic transport on the dislocation movement and local microstructure evolution, especially in the early stage of electromigration, is unclear.

Recently, with the development of new experimental techniques, it becomes possible to measure precisely the change in grain orientation and local stress with a lateral resolution compatible with the length scale of the interconnects (i.e. the scale of

their constitutive grains) [7, 8]. Very small submicron high brilliance X-ray beam can be produced using focusing optics such as Kirkpatrick-Baez (KB) mirrors at synchrotron facilities [8,9] and advanced diffraction techniques using them, such as synchrotron based polychromatic (white) X-ray microdiffraction, have especially been proven to be ideal tools for interconnect reliability study [10,11]. In the latter technique, data are rapidly recorded as a raster scan array of Laue diffraction patterns (LPs) by a large area charge coupled device (CCD) X-ray detector and analyzed to obtain stress and texture maps of the sample with a resolution only limited by the size of the focused X-ray beam. This tool can also be used to map plasticity effects at submicron level.

Previous works on Al (0.5 wt % Cu) or Cu damascene interconnects showed the potential of Laue X-ray microdiffraction to map grain orientation [7], study plastic deformation [12-15] and dislocation arrangement [16] induced by electromigration. In the present paper, we report a more in-depth study on grain deformation and rotation along the Al (0.5 wt % Cu) interconnect during the early stage of electromigration and the characterization of the active dislocations slip systems in function of stress.

II. Experimental

The sample used for the electromigration test was a sputtered Al (0.5 wt % Cu) two-level structure with the dimensions of 4.1 μm in width, 30 μm in length, and 0.75 μm in thickness. Two Ti layers, one layer at the bottom of the Al line with 450 Å thick and the other on the top of the Al line with 100 Å thick, were used as shunt; and a 0.7 μm thickness SiO_2 layer was used as passivation. Electrical connection between this Al line to unpassivated Al (Cu) pads was achieved by several W vias at either end. Before

current stressing, the sample was annealed at 390 ^{o}C for 30 min in a vacuum about 10^{-5} torr.

The *in-situ* X-ray microdiffraction experiment has been conducted on Beamline 7.3.3 at the Advanced Light Source synchrotron in Berkeley, CA. The beamline configuration and capabilities have been described elsewhere [17]. The chip carrier containing the wire-bonded sample was mounted at 45^{o} incidence with respect to the beam and Laue diffractions produced by a KB focused submicron size (0.7 x 0.7 um^2) white beam from a bend magnet hitting the sample were recorded by a Bruker6500 CCD detector mounted at 90^{o} with respect to the beam and at about 5 cm above the sample.

The electromigration test was conducted at a constant temperature by setting the heater temperature at 224 ^{o}C and the current density was ramped up to 0.98×10^6 A/cm^2 (I = 30 mA) and maintained constant for a period of 25 hours. Then the current direction was reversed but kept at the same magnitude for another 20 hours. Before and during the electromigration test, X-ray microdiffraction LPs were recorded by scanning the sample repeatedly by a micron-sized white beam. When scanning the sample, each step size was set as 0.5 μm, so 15 steps across the width of the line and 65 steps along the length were needed to cover the whole surface of the sample for each scan, which includes totally 975 CCD frames. The CCD exposure time was set to be 5 seconds and the electronic readout time for each frame was about 10 seconds. As a result, for each scan, it took about 4 to 5 hours. The Laue diffraction data were analyzed using the custom written XMAS software [12, 18]. The orientation of each grain was expressed by a 3×3 matrix.

III. Results and discussion

1. Dislocation active slip systems

When subjected to the high current density, bending and ultimately polygonization [11] are observed in large grains, especially those that span across the width of the line ("bamboo" type) when a certain yield stress is reached.

This aspect of EM-induced plastic deformation in grains results in the broadening of the Laue spots along certain directions, compatible with the bending direction. It is due to the arrangement of excess geometrically necessary dislocations (GNDs) [19]. When same-sign dislocations are introduced into a material, the lattice planes will appear bent at a mesoscopic scale. Scattering takes place at different angle and wavelength in different parts of the material according to Bragg's law. With the use of a polychromatic beam, Bragg's law is satisfied for a large range of lattice bending and the diffraction peak is observed as a streak. The streaking direction provides the direction of the bending. Analysis of the Laue spot broadening patterns allows for the identification of the active dislocation slip system that produced the bending.

Fig. 1 (a) shows a typical Laue diffraction pattern recorded after about 12 h of EM test. The strong Laue peaks indicated by white arrows in the LP are the diffraction peaks from the Si substrate, while the other weak peaks are from Al. These Al diffraction peaks have been indexed by the software XMAS, and orientation information obtained. In order to study the plastic deformation on the Al line, some of the Al peaks have been zoomed in so that the peak shape can be studied in more details. **Fig. 2** (a) – (l) show the simulated LPs obtained from the Al crystal oriented in the same way as the crystal grain shown in **Fig. 1** (a) and subjected to each of the 12 most possible {111}/<110> edge

dislocation slip systems for a FCC metal. Comparing these simulated LPs with the one in **Fig. 1** (a), the best match is **Fig. 2** (c), in which the slip plane is along (111) plane, the slip direction is along $[0\bar{1}1]$ direction, and the dislocation line direction is along $[\bar{2}11]$ direction. Practically all slip systems with screw dislocations have also been simulated but the resulting LPs do not match **Fig. 1** (a). **Fig. 1** (b) represents the stereographic projection of this grain which contains all the possible dislocation directions. One noticeable observation is that the $[\bar{2}11]$ direction is the closest to the current flow direction among the <211> family.

The slip systems in thirty grains have been analyzed by this method. All the dislocations are found to be edge typed and about 90 % of the dislocation lines are contained within 5^{o} with respect to the current flow direction, and the 10 % which don't obey this rule are located close to the cathode end of the Al line. We propose that the dislocations are aligned in this way to minimize the electrical resistance because of the anisotropy of the scattering between electrons and dislocations. Much effort has been made to calculate the contribution of dislocations to electric resistivity [20-22]. These efforts show that, in single crystals, the resistance opposed by dislocations in the direction parallel to the dislocation lines is zero, while the resistance in the slip direction exceeds the resistance normal to the slip plane by a factor of about 2 for aluminum. The dislocations at the cathode end are not aligned because electrons enter the Al line here and the electron motion directions are more disordered in this region. The realignment of dislocations will also influence the atomic diffusion inside the Al line by affecting the diffusion route. The details of the kinetic study will be the subject of a forecoming paper.

2. Shear force analysis

By analyzing the deviation of the Laue peak positions from their ideal positions scattered by an unstrained crystal, distortional strain/stress tensor can be obtained with high accuracy [12]. However, in the present case, strain/stress cannot be accurately measured by this method because, as stated before, the Laue peaks are streaked due to the bending of the grains induced by EM, so that it is very difficult to determine precisely the peak positions. Furthermore, since the X-ray beam has a certain spot size, rather than an ideal spot, there is strain gradient, as well as orientation gradient, within the irradiated volume of the sample. As a result, we developed a new method to estimate the shear stress based on Schmidt's law.

According to Schmidt's law, a slip system can be activated only if a certain critical value of the resolved shear stress is reached. The magnitude of resolved shear stress is a function of the applied stress, the orientation of the slip plane, and of the slip direction within the plane. Let ϕ represent the angle between the force direction and the normal to the slip plane, and λ the angle between the force direction and the slip direction. The Schmidt factor is defined as:

$$F_s = \cos\phi \cos\lambda .$$

When a force is applied on a single crystal, F_s can be calculated for each slip system, and the one with the highest Schmidt factor is the most favorably oriented and the most likely being activated. Based on this assumption, force direction can be

estimated within a certain error margin if the most favorable slip system and the orientations of each slip plane and slip directions are known.

For example, for a given grain in the Al line, the force direction can be written as:

$\vec{\mathbf{d}}_F = \cos\alpha\bar{\mathbf{x}} + \cos\beta\bar{\mathbf{y}} + \cos\gamma\bar{\mathbf{z}}$,

where the unit vectors $\bar{\mathbf{x}}$, $\bar{\mathbf{y}}$, and $\bar{\mathbf{z}}$ are respectively along the current flow direction, across the line width, and normal to the line surface, , and α, β, γ are the angles between the force vector and respectively the unit vector $\bar{\mathbf{x}}$, $\bar{\mathbf{y}}$, and $\bar{\mathbf{z}}$, so that:

$$\cos^2\alpha + \cos^2\beta + \cos^2\gamma = 1.$$

Since the orientation of the grain is known by indexing the LP, the Schmidt factor of each slip system can be calculated by inputting a set of $\cos\alpha$, $\cos\beta$, and $\cos\gamma$ values. We also know which slip system has been activated by analyzing the Laue peak shape as described above. By adjusting the values of $\cos\alpha$, $\cos\beta$, and $\cos\gamma$, an interval can be obtained within which the activated slip system has the highest Schmidt factor among all the twelve {111}/<110> possibilities for a FCC structure.

However, this method cannot make the distinction between a tensile and a compressive force, because the same slip system can be activated by both, as long as the stress exceeds the critical resolved shear stress. The force directions have been estimated for 20 grains located at the cathode end of the sample, where we assume all the grains are under tensile stress after EM stress. **Fig. 3** summarizes the distribution of the shear force as a function of the distance from the center of the grain to the center of the Al line width.

Note that according to the classic theory, there is a pair of shear forces to active a slip with opposite direction; however, here in **Fig. 3** we only consider the shear force with positive $\bar{\mathbf{z}}$ components. The shear force analysis shows that the force components along the $\bar{\mathbf{y}}$, and $\bar{\mathbf{z}}$ directions strongly depend on the distance from the center of the grain to the center of the Al line width, as shown in **Fig. 3** (a, b). The $\bar{\mathbf{y}}$ components of the forces applied on the grains at different side of the Al line are in opposite directions (have opposite signs), and the $\bar{\mathbf{y}}$ force components always point towards the center of the line. The grains at the center suffer the forces that is almost perpendicular to the line surface (pure $\bar{\mathbf{z}}$ component), while the grains at the edge suffer the forces with much larger $\bar{\mathbf{y}}$ or $-\bar{\mathbf{y}}$ components. We propose that the shear force on each individual grain is produced from the tensile stress caused by EM and the interactions with its neighboring grains, while the grains in the center are subjected upon the forces with opposite signs from the two halves across the width and they cancel each other, so only $\bar{\mathbf{z}}$ component is left.

3. Grain rotation

Besides bending, grain rotation induced by EM was primarily observed in grains that do not span the total width of the line (non "bamboo" grain) [11]. It was found that grains situated on opposite sides across the width of the line rotated in opposite directions and that the farther the grain was lying from the anode side, the larger was the rotation. A mechanism has been proposed to explain the resulting concave bowing of the line at the cathode end [13]. Here, we conducted a more thorough study of 48 grains out of a total of 55 grains detected in the Al line. Rotation angle, as well as the rotation axis, is precisely derived from the orientation matrices computed from the LPs, with respect to

the initial orientation matrix before EM. For example, the orientation matrices of Grain G before and after EM test are A and B, respectively. The rotation matrix, $R = BA^{-1}$, contains the information of both rotation angle and rotation axis. The results are summarized in **Fig. 4**. **Fig. 4** (a) shows the evolution of rotation after 12 hr and 25 hr of electromigration. Although the initial study indicated a seemingly almost linear dependence of the rotation angle as a function of the position along the line, the now more complete set of data showed that rotation becomes large at a position situated approximately one third of the total length of the line starting from the anode end. Also it shows that all the grains have rotated further after 25 hr current stressing compared to 12 hr in the same direction. **Fig. 4** (b) is a linear fit of the rotation angle as a function of time. The slope is 1.92, which means that in average, the grains rotated linearly with time during the early stage of electromigration test.

Two main reasons may contribute to the slower rotation rate of the grains at the anode end than the ones at the cathode end. First, when EM test is performed on Al (Cu) interconnect lines, the anode end is hardened because Cu is pushed from the cathode to the anode prior to Al due to higher diffusivity [23-25] so that Cu is concentrated in this region. The higher hardness results in the smaller plasticity and smaller grain rotation. The other reason is that since the atoms are pushed to the anode side, which is under compressive stress, from the cathode end, which is under tension, the vacancy concentration at the cathode is higher than the anode. As well known, substitutional diffusion is vacancy assisted, so the atoms can move faster at the cathode than at the anode [26]. Detailed quantitative modeling is hard for the kinetic analysis of the grain

rotation procedure because of the complicated environment of each individual grain and the interactions with its neighboring grains.

Besides the rotation angle, the rotation axis around which grain rotation occurs can be computed from the orientation matrices before and during EM. Since grains on either side of the Al line rotate in opposite directions, rotation axes for either side are anti-parallel. The arrows drawn in **Fig. 5** (a) are parallel to the projection of the rotation axis in the plane of the sample and the length of the arrow represents the magnitude of the rotation. The color code refers to the cosine of the angle α between the rotation axis and the current flow (blue: $\cos\alpha \approx -1$, red: $\cos\alpha \approx 1$). **Fig. 5** (b) shows the representation of $\cos\alpha$ as a function of the grain position across the line. Most dots in **Fig. 5** (b) have the value of 1 or -1, which means that most of the rotation axes are either parallel or anti-parallel to the current flow direction. The dots in the center of the line have cosine values between 1 and -1, indicating a more random distribution. Some of these grains that have a barycenter in the middle are actually "bamboo" type grains. These large grains are subject to opposite stress moments at opposite sides across the lines, so that the net rotation might indeed be very small compared to what is observed for smaller grains situated at edges. Another important observation is that there are less data points after 25 hours that deviate from 0^o or 180^o, which means that the longer time the sample is stressed by current flow, the more grains inside the sample will rotate along the current flow direction, resulting in a binomial distribution.

4. Quasi-quantitative modeling of concave and rotation angles

The shear stress distribution as in the cross section of the Al interconnect line at the cathode end is schematically shown in **Fig. 6** (a). Since the adhesion between the Al line and the substrate is strong and the Al line is constrained by the substrate, it is assumed that the shape of the Al atomic plane doesn't change at this interface. However, the planes are curved at the Al line / passivation layer interface, and the displacement direction is schematically shown in **Fig. 6** (b). By measuring the rotation angle of the grain at every spot in the cross section, the curvature of the plane can be calculated.

As a quasi-quantitative model, first we a two-dimensional array of atoms is generated with the aspect ratio 4 : 0.75, which is approximately the same as the cross section of the testing sample, as the black dot array shown in **Fig. 6** (c). Then displacement is applied to each of the atoms. Since the atoms in the bottom layer are constrained by the substrate, their displacement is 0. We assume the magnitude displacement of each atom obeys the following equation:

$$\delta = Ayx^2 + By$$

where A and B are constants, x and y are the coordinates of the atom along the width and thickness directions, respectively, and the direction of the displacement on each atom is pointing towards the origin of the coordinates. This displacement field generates a concavity of the atomic layers compatible with the measured curvature. Based on this model, the atom positions are indicated by the red dots in **Fig. 6** (c). In this image the atomic layers are concaved as we expected, and the curvature is controlled by the factors A and B.

The fitting of the model to the experimentally observed curvature allows determining the constants A and B and thus the shape of cross section. To achieve this, the tangent values of the rotation angles of 30 grains after 12 hr electric current stressing are recorded as a function of the barycenters of these grains along the width direction. All these grains are located more than 10 μm away from the anode end because as shown above in **Fig. 4** (a), the rotation angles in this region are basically dependent on the distance along the width direction, rather than along the current flow direction. The results are shown by the blue dots and error bars in **Fig. 6** (d). The factors A and B are adjusted and when the displacement magnitude function is $\delta = \frac{1}{31} yx^2 + \frac{1}{80} y$, the curvature of the top atomic layer fits the experimental data points reasonably as shown by the red dots and line in **Fig. 6** (d). Define the strain in the width direction ε_{yy} and in the thickness direction ε_{zz} as

$$\varepsilon_{yy} = \frac{\delta y}{|y|}$$
$$\varepsilon_{zz} = \frac{\delta z}{0.75\mu m}$$

where δy, δz are the atomic displacement in the width and thickness directions, respectively, and $|y|$ is the distance from the certain atom to the middle of the Al line. The distributions of the strains in the two directions of the top atomic plane are shown Fig. (e) and (f) respectively. ε_{yy} is negative and ε_{zz} is positive, and the magnitude ranges from about 1% to 5%, which is much larger than the elastic limit. It is also

noticeable that the strain magnitude at the edge of the line is 4 – 5 times as high as in the middle.

IV. Summary

By using polychromatic X-ray beam microdiffraction, we have studied the microstructure evolution of each individual grain in an Al (Cu) interconnect line stressed by electrical current at the early stage of EM. From the shape of the Laue spots, bending in large grains has been analyzed; the position shift of the Laue spots provides grain rotation information which happens in small grains. The activated slip system, as an index of plastic deformation, is determined by theoretical simulation for many grains and it is summarized that the GNDs with the dislocation line direction parallel to the current flow direction are always preferentially activated, which is believed to be the most electrical conductance preferred orientation. Also from the slip system, shear stress direction is obtained. In this EM experiment, shear force distribution is revealed as a function of the distance from the center of the Al line, which helps us understand the phenomenon of grain rotation caused by the concave of the line.

Acknowledgements: The Advanced light Source is supported by the Director, Office of Science, Office of Basic Energy Sciences, of the U.S. Department of Energy under Contract No. DE-AC02-05CH11231 at Lawrence Berkeley National Laboratory

References:

1. I. A. Blech, J. Appl. Phys. **47**, 1203 (1976)
2. K. N. Tu, J. Appl. Phys. **94**, 5451 (2003)
3. S. Vaidya, and A. K. Sinda, Thin Solid Films **75**, 253 (1981)
4. P. S. Ho, and T. Kwok, Rep. Prog. Phys. **52**, 301 (1989)
5. M. A. Korhonen, P. Borgesen, K. N. Tu, and C. Li, J. Appl. Phys. **73**, 3790 (1993)
6. H. Gan, K. N. Tu, J. Appl. Phys. **97**, 063517 (2005)
7. N. Tamura, A. A. MacDowell, R. S. Celestre, H. A. Padmore, B. C. Valek, J. C. Bravman, R. Spolenak, W. L. Brown, T. Marieb, H. Fujimoto, B. W. Batterman, and J. R. Patel, Appl. Phys. Lett. **80**, 3724 (2002)
8. O. Hignette, P. Cloetens, G. Rostaing, P. Bernard, C. Morawe, Rev. Sci. Instrum. **76**: Art. No. 063709 (2005)
9. W. J. Liu, G. E. Ice, J. Z. Tischler, A. Khounsary, C. Liu, L. Assoufid, A. T. Macrander, Rev. Sci. Instrum. **76**: Art. No. 113701 (2005)
10. P. C. Wang, G. S. Cargill III, I. C. Noynan, and C. K. Hu, Appl. Phys. Lett. **72**, 1296 (1998)
11. B. C. Valek, J. C. Bravman, N. Tamura, A. A. MacDowell, R. S. Celestre, H. A. Padmore, R. Spolenak, W. L. Brown, B. W. Batterman, and J. R. Patel, Appl. Phys. Lett. **81**, 4168 (2002)
12. N. Tamura, H. A Padmore, and J. R. Patel, Mater. Sci. Eng. A, **399**, 92 (2005)
13. B. C. Valek, N. Tamura, R. Spolenak, W. A Caldwell, A. A. MacDowell, R. S. Celestre, H. A. Padmore, J. C. Bravman, B. W. Batterman, W. D. Nix, and J. R. Patel, J. Appl. Phys. **94**, 3757 (2003)

14. A. S. Budiman, N. Tamura, B. C. Valek, K. Gadre, J. Maiz, R. Spolenak, J. R. Patel, and W. D. Nix, Mater. Res. Soc. Symp. Proc. 914 (2006)

15. R. I. Barabash, G. E. Ice, N. Tamura, B. C. Valek, J. C. Bravman, R. Spolenak, and J. R. Patel, J. Appl. Phys. **93**, 5701 (2003)

16. A. S. Budiman, W. D. Nix, N. Tamura, B. C. Valek, K. Gadre, J. Maiz, R. Spolenak, J. R. Patel, Appl. Phys. Lett. **88**, 233515 (2006)

17. N. Tamura, A. A. MacDowell, R. Spolenak, B. C. Valek, J. C. Bravman, W. L. Brown, R. S. Celestre, H. A. Padmore, B. W. Batterman and J. R. Patel, J. of Synchrotron Radiat. **10**, 137 (2003)

18. N. Tamura, R. Spolenak, B. C. Valek, A. Manceau, M. Meier Chang, R. S. Celestre, A. A. MacDowell, H. A. Padmore, J. R. Patel, Rev. Sci. Instrum. **73**, 1369 (2002)

19. H. Gao, and Y. Huang, Scripta Mater. **48**, 113 (2003)

20. J. K. Mackenzie, and E. H. Sondheimer, Phys. Rev. **77** (2), 246 (1950)

21. R. A. Sacks, and J. E. Robinson, Phys. Rev. B **13** (2), 611 (1976)

22. H. Bross, and O. Häberlen, J. Phys. Condens. Matter **5**, 7687 (1993)

23. C. -K. Hu, M. B. Small, and P. S. Ho, J. Appl. Phys. **74**, 969 (1993)

24. C. -K. Hu, Thin Solid Film **260**, 124 (1995)

25. H. -K. Kao, G. S. Cargill, and C. -K. Hu, J. Appl. Phys. **89**, 2588 (2001)

26. D. A. Porter, and K. E. Easterling, *Phase transformations in metals and alloys*, (Chapman & Hall, New York, 1992)

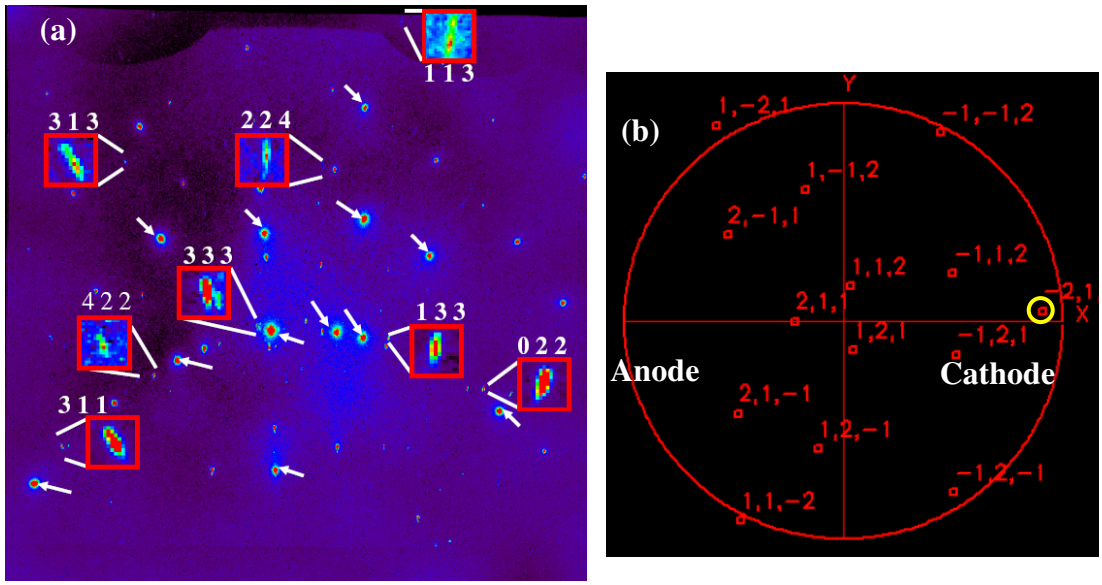

Fig. 1 (a) Laue diffraction pattern recorded after 12 hr EM test, and (b) the stereo projection of the same grain (y is across the Al line width direction and x is the electrical current flow direction)

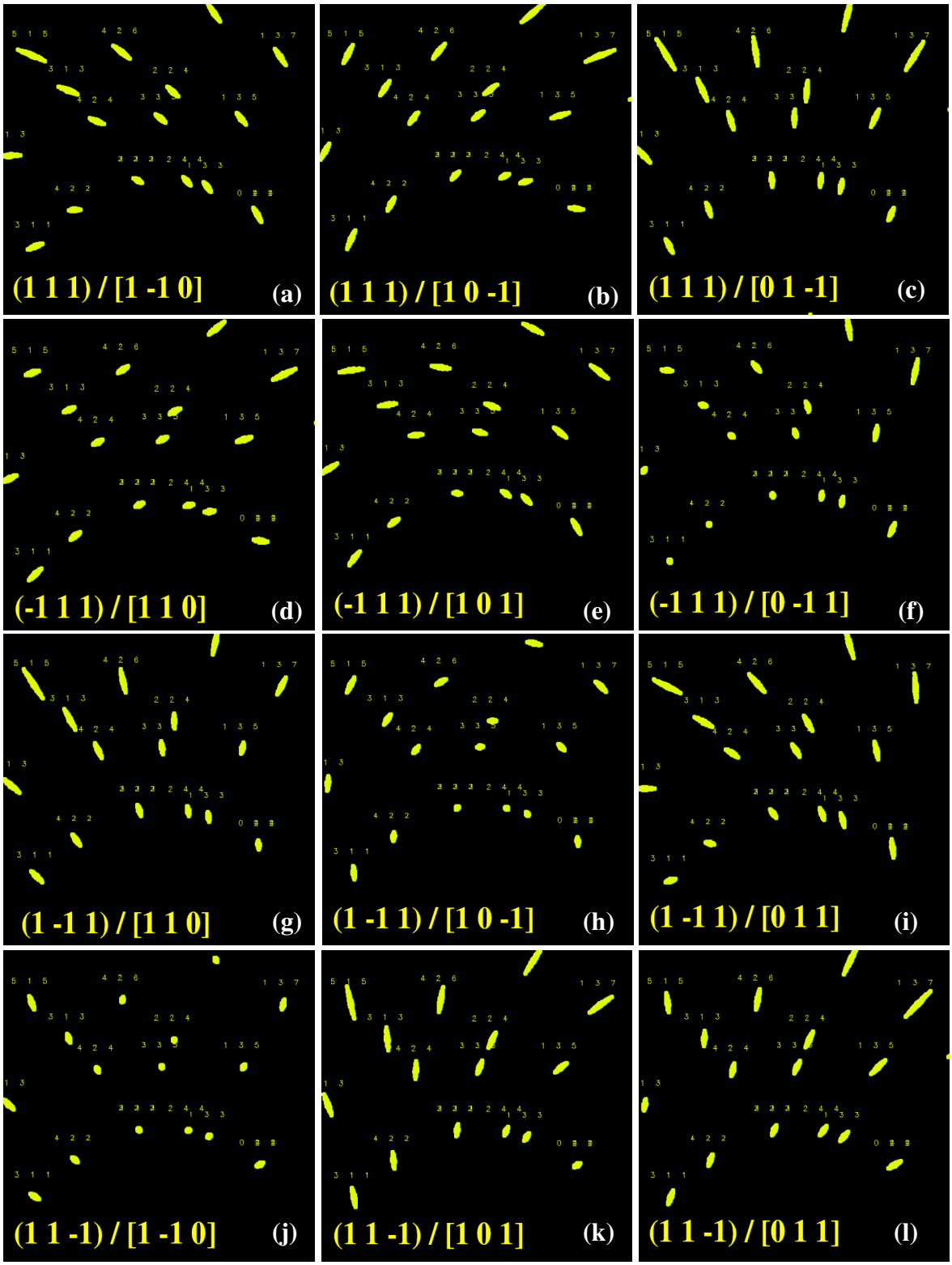

Fig. 2 (a) – (l) simulated Laue patterns with 12 each of the most possible slip systems in Al crystal with the same orientation as the grain in **Fig. 1**

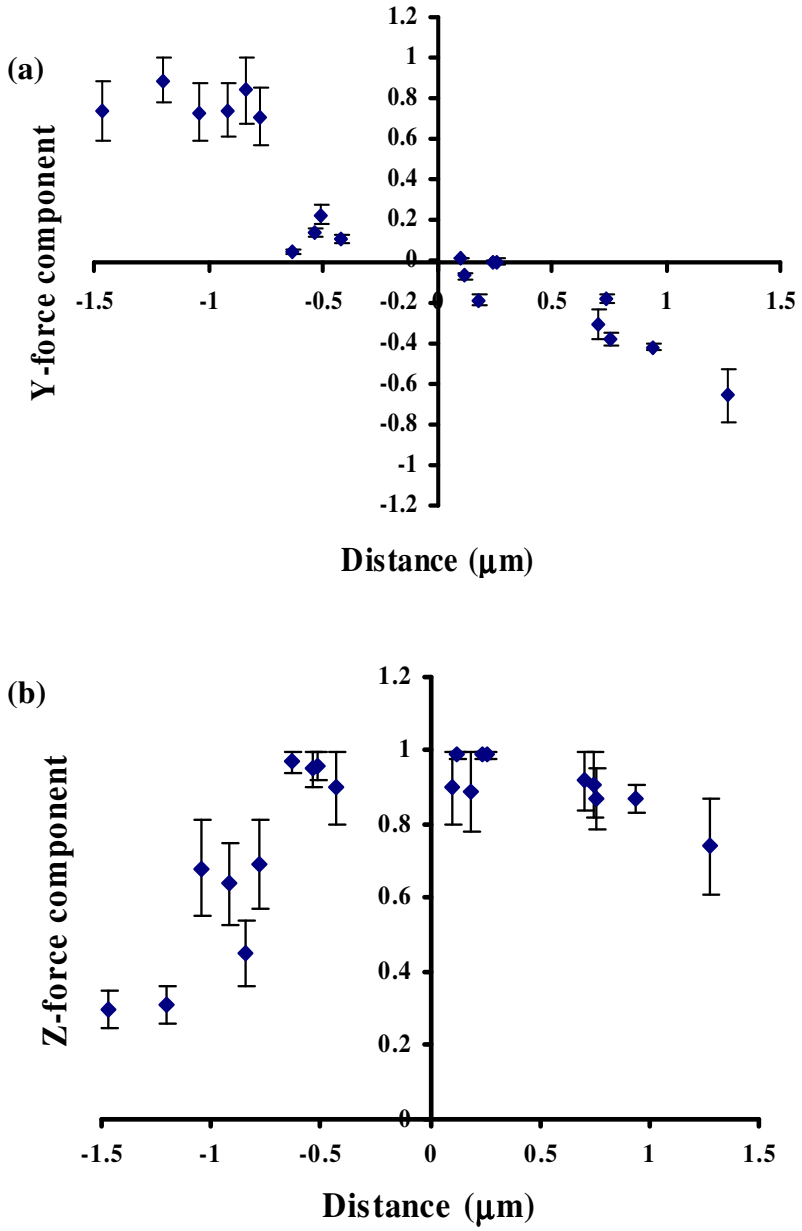

Fig. 3 Force in (a) y direction and (b) z direction as a function of the distance from the center of the grain to the middle of the Al line width.

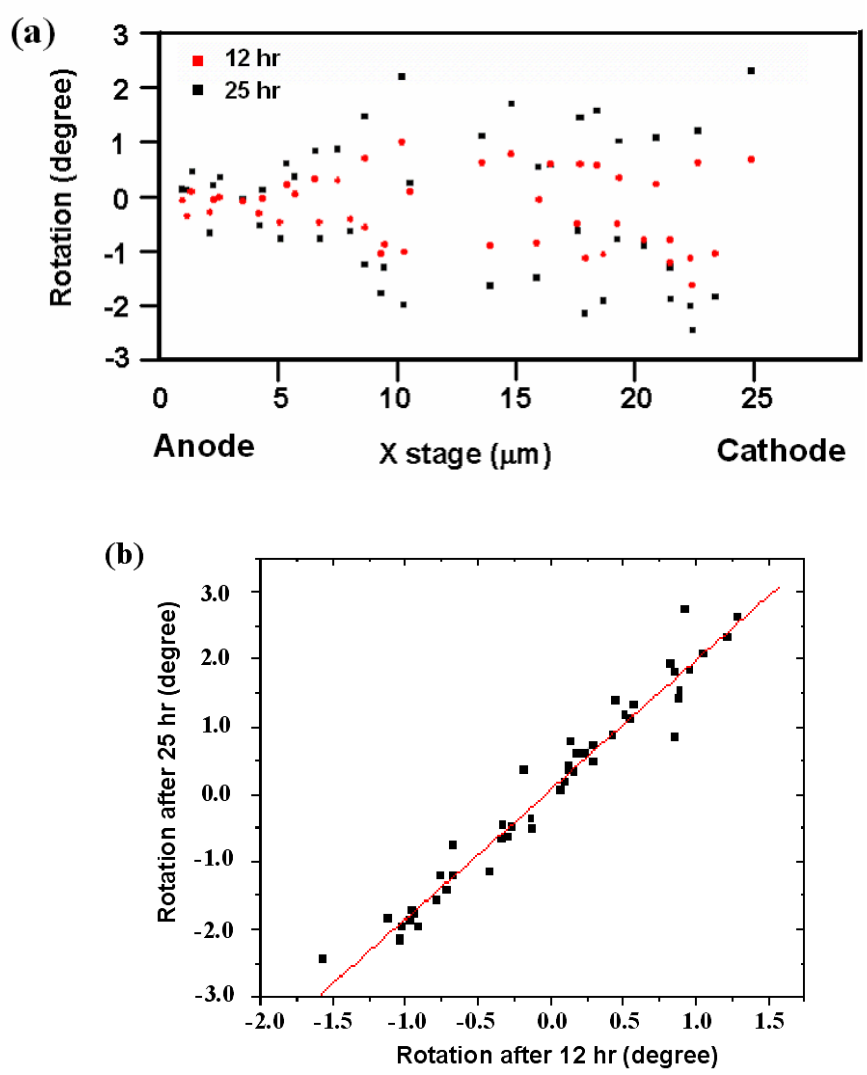

Fig. 4 Grain rotation angle distribution and evolution during EM (a) grain rotation angles at different positions (Anode is on the left and cathode on the right) after electromigration tests for 12 hr and 25 hr (b) linear fit of gain rotation angle evolution in a period of 13 hr

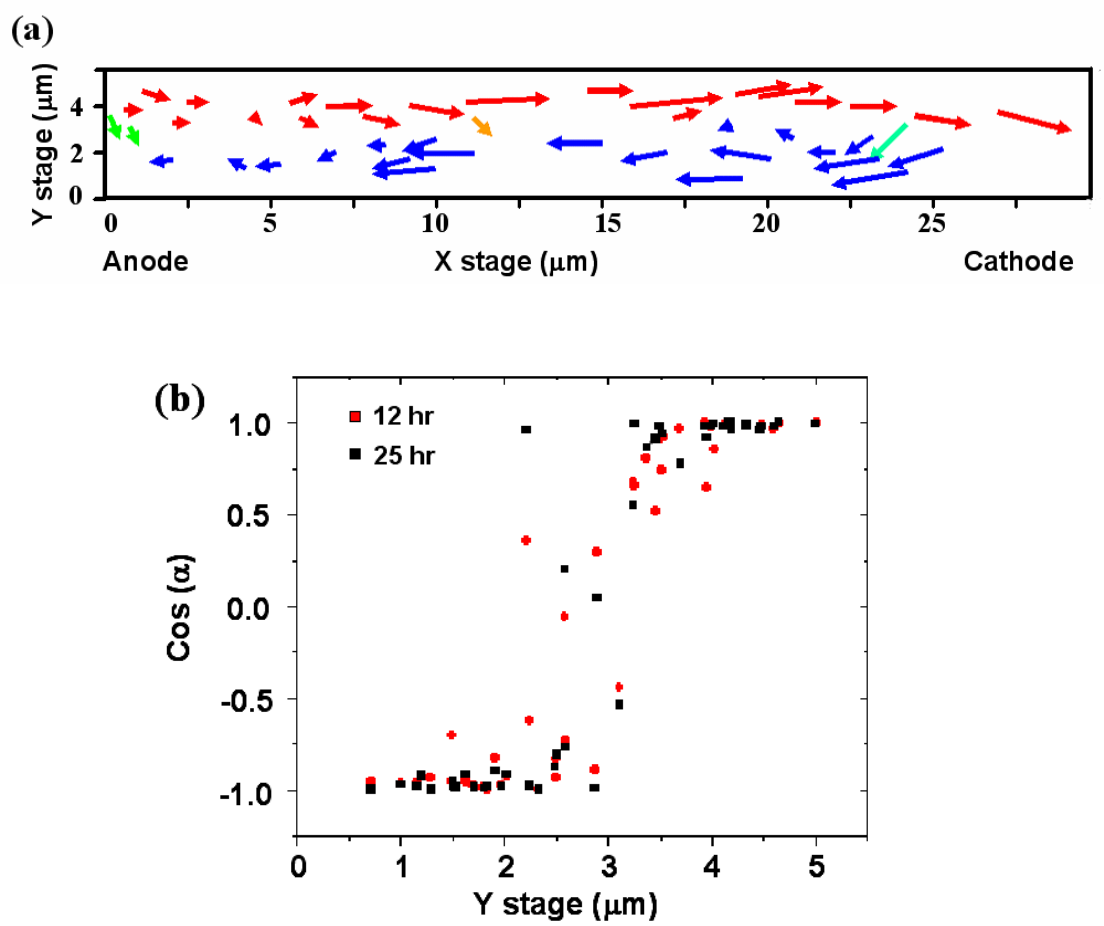

Fig. 5 (a) The projection of rotation axes on the Al interconnect line plane, and (b) quantitative analysis of rotation axis directions after 12 hr and 25 hr EM test, respectively

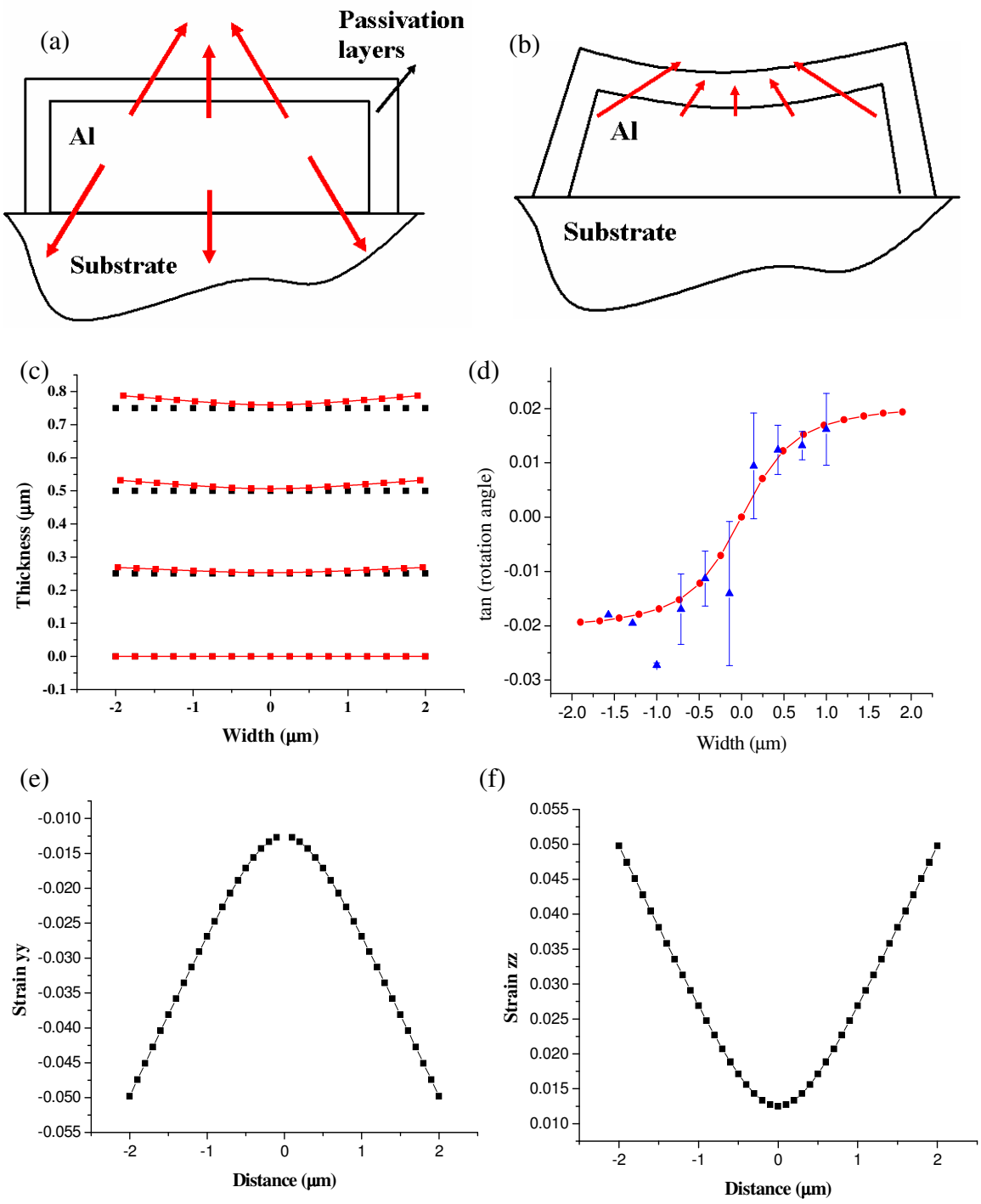

Fig. 6 Schemes of the (a) shear force distribution and (b) displacement direction, (c) an array of atoms before and after strain application, (d) the curvature of the Al line surface, and the distributions of the strains in (e) width and (f) thickness direction